GRASPING

In situ foliar augmentation of multiple species for optical phenotyping and bioengineering using soft robotics

Mehmet Mert İlman[1,2], Annika Huber[3]†, Anand K. Mishra[1]†, Sabyasachi Sen[1], Fumin Wang[4], Tiffany Lin[3], Georg Jander[4], Abraham D. Stroock[3,5,6], Robert F. Shepherd[1]*

Precision agriculture aims to increase crop yield while reducing the use of harmful chemicals, such as pesticides and excess fertilizer, using minimal, tailored interventions. However, these strategies are limited by factors such as sensor quality, which typically relies on visual plant expression, and the manual, destructive nature of many nonvisual measurement methods, including the Scholander pressure bomb. By automating more intimate interactions with foliage in vivo, it would be possible to inject chemical and biological probes that reveal more phenotypes—such as water stress in response to varying environmental conditions and visible gene expression to measure the success of gene engineering applications. To address this, we developed a soft robotic leaf gripper and stamping-injection method to improve foliar delivery of nanoscale synthetic and biological probes. This allows for nondestructive, in situ, multispecies applications. We used two probes: *Agrobacterium tumefaciens* carrying the *RUBY* gene as a reporter system for plant transformation and nanoparticle hydrogels for measuring leaf water potential (ψ). Our hourglass-shaped design enabled the gripper to exert higher forces with reduced radial expansion compared with conventional designs, achieving an injection success rate above 91%. Studies on sunflower (*Helianthus annuus* L.) and cotton (*Gossypium hirsutum* L.) showed that our method achieved an average 12-fold increase in infiltration areas, with substantially less leaf damage—3.6% in sunflower and none in cotton—compared with the needle-free syringe method. Enabling long periods of successful in vivo phenotyping on both species after precise and safe foliar delivery underscores the potential of the leaf gripper for robotic plant bioengineering.

INTRODUCTION

Precision agriculture shows promise in addressing food security challenges posed by political and environmental issues and population growth (*1*). However, slow progress in agricultural robotics and automation may be delaying the realization of its full potential. Advancements in precision agriculture technologies are vital for achieving the goal of making every food product controllable and trackable throughout production (*2*). This advance could help environmental safety and economic sustainability by minimizing the unnecessary use of resources, fertilizers, and pesticides (*3*).

Current precision agriculture technologies can be categorized on the basis of phenotyping levels and measurement ranges. Remote phenotyping applications, for example, are used to detect insect infestations (*4*) and weeds (*5*); to predict yield (*6*); and to assess plants (*7*), soil (*8*), and environmental conditions (*9*). However, this approach remains limited in specificity, accuracy, and biological detail (*3*). In contrast, contact-based phenotyping enables more precise and localized measurements through plant wearables (*10*) and robotic grippers for stress detection (*11*), fluorescence (*12*), and ripeness assessment (*13*). Although this method offers greater detail, its effectiveness is limited by the number of available biomarkers. Meanwhile, in vivo phenotyping leverages injectable plant bioengineering technologies, such as genetic engineering for endophenotyping or nanoparticles as biosensors for monitoring physiological changes (*14*). Incorporating nanotechnology and genetics offers the potential to harness and modify plants, creating biohybrids that are ultimately carbon negative (*15*).

Foliar delivery plays a crucial role in in vivo phenotyping and precision agriculture by enabling the direct, localized application of agrochemicals, nanoparticles, and genetic materials to plant tissues with high efficiency. Unlike soil-based delivery, which can lead to nutrient leaching and environmental contamination, foliar infiltration ensures targeted treatment with minimal waste (*16*). For instance, live-cell imaging using fluorescent proteins (*17*) has enabled visualization of damage signaling pathways in *Arabidopsis thaliana* (*18*). Leuzinger *et al.* (*19*) used *Agrobacterium tumefaciens* as a foliar delivery mechanism for the transient expression of green fluorescent protein in tobacco (*Nicotiana benthamiana*). Similarly, He *et al.* (*20*) introduced the *RUBY* gene, which produces ruby-colored pigmentation, serving as a naked-eye visual reporter for transgenic plants. Beyond genetic engineering, foliar delivery also enables real-time physiological monitoring. Jain *et al.* (*21*) used hydrogel nanoparticles (AquaDust) to continuously track leaf water potential (ψ) in maize (*Zea mays L.*). In addition, nanoparticles can extend plant functionalities; Wong *et al.* (*22*) demonstrated how engineered spinach plants (*Spinacia oleracea L.*) could detect explosive molecules, emitting infrared signals that were easily intercepted using a smartphone camera.

Despite their promise, foliar delivery methods have yet to reach their full potential because of three key challenges in leaf infiltration resistance (Fig. 1B). One major factor is the stomatal aperture [*a* (in micrometers)], the pore opening in leaves that regulates transpiration and carbon dioxide (CO_2) uptake (*23*). Plants adjust it between 0 and 20 μm on the basis of light, drought stress, and humidity, potentially limiting foliar delivery (*24*). Another challenge is hydrophobicity,

[1]Sibley School of Aerospace and Mechanical Engineering, Cornell University, Ithaca, NY 14853, USA. [2]Department of Mechanical Engineering, Hasan Ferdi Turgutlu Faculty of Technology, Manisa Celal Bayar University, Manisa 45400, Türkiye. [3]Smith School of Chemical and Biomolecular Engineering, Cornell University, Ithaca, NY 14853, USA. [4]Boyce Thompson Institute, Ithaca, NY 14853, USA. [5]School of Integrative Plant Science, Cornell University, Ithaca, NY 14853, USA. [6]Kavli Institute at Cornell for Nanoscale Science, Cornell University, Ithaca, NY 14853, USA.
†These authors contributed equally to this work.
*Corresponding author. Email: rfs247@cornell.edu

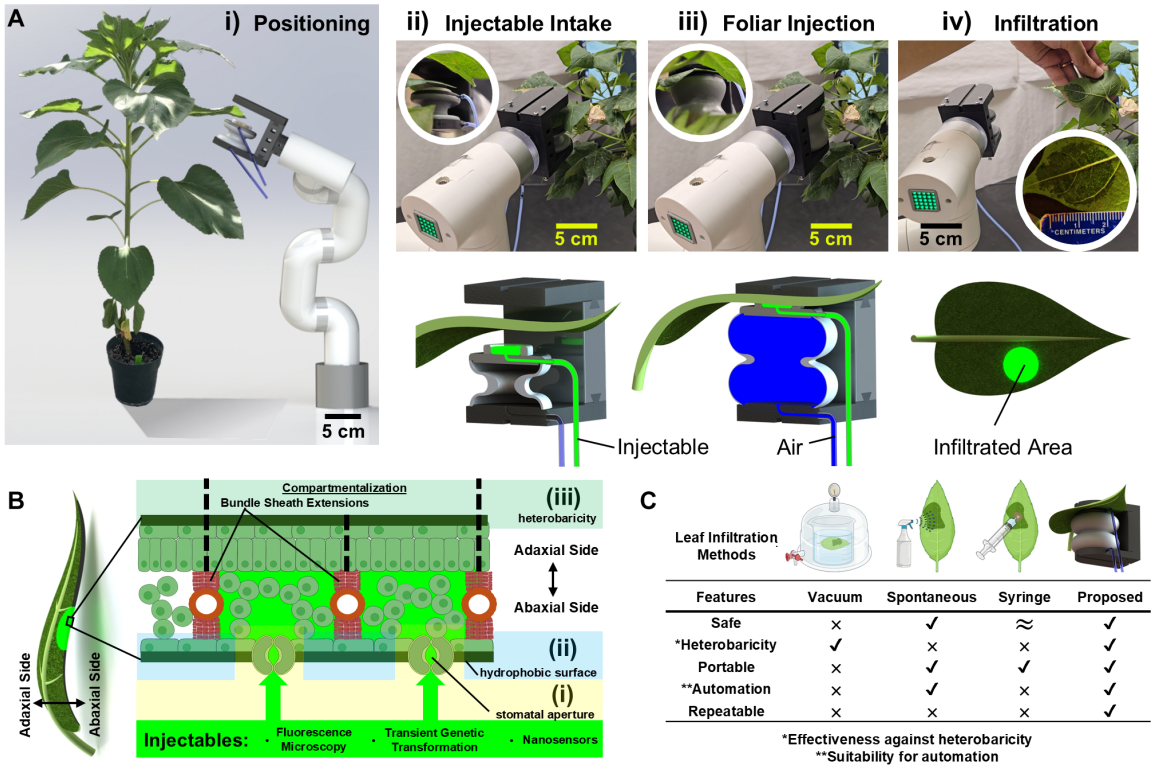

Fig. 1. Automated foliar delivery with the leaf gripper. (**A**) Robot arm demonstration: (i) positioning with manipulator, (ii) automated injection preparation with liquid pump, (iii) foliar delivery by stamping with air pump, and (iv) releasing the leaf and showing the infiltrated area. Scale bars, 5 cm. (**B**) Leaf cross section and infiltration resistance mechanisms: (i) small stomatal aperture, (ii) hydrophobic surfaces, and (iii) heterobaricity. (**C**) Comparison of the proposed method with benchmark foliar delivery methods: vacuum chamber, spraying, and needle-free syringe. ≈ denotes the syringe method as generally safe, although shear forces may sometimes cause tearing beyond minor injury, especially in heterobaric leaves.

driven by the leaf's waxy cuticle and stomatal pores. This property repels water, reducing microbial growth but creating capillary stresses that hinder infiltration (*25*). A third challenge is heterobaricity, defined by bundle sheath extensions (BSEs) that separate intercellular air spaces. Heterobaricity reduces microbial spread, enhances mechanical stability, and can restrict infiltrated liquid movement (*26*, *27*). Many model plants, including sunflower, soybean, cotton, and wild tomato, exhibit heterobaricity, which can enhance survival by improving resistance to drought and wind; however, genetic modifications can minimize BSEs and this trait (*25*).

Current approaches to foliar delivery include spontaneous infiltration, vacuum chambers, and needle-free syringes (*28*). Spontaneous infiltration is limited by leaf hydrophobicity, which surfactants can reduce, although only at low concentrations to prevent cell membrane damage (*29*, *30*). Forced infiltration methods, such as vacuum infiltration, can be more efficient by removing air pockets in the apoplast and replacing them with liquid in heterobaric leaves (*31*). However, this method requires submerging the leaf in liquid, limiting portability and control over the injected area and leading to patchy infiltration (fig. S2A). This affects in vivo phenotyping, such as agroinfiltration, where high substance distribution is crucial for overcoming immune responses and ensuring infection, or AquaDust injection, where lower density reduces fluorescence intensity. The needle-free syringe method, although injuring the injection site, is the most practical method for delivering substances across homobaric leaves with interconnected air spaces (*28*). Koman *et al.* (*32*) showed that automating this method improves reliability and supports plant nanobionics. However, in medium to highly heterobaric leaves, its effectiveness decreases because the injury often surpasses the spread area (figs. S1 and S2C).

Here, we introduce a simple, versatile, and adaptable soft robotic gripper with a previously unreported automated stamping-based foliar delivery method (Fig. 1A, Movie 1, and movies S1 and S2) that can delicately handle leaves without notable injury while being robust against anatomical features such as heterobaricity and variable stomatal aperture (Fig. 1B) across different plants, unlike conventional counterparts (Fig. 1C). Soft grippers have been successful in safely handling living creatures (*33*, *34*); however, existing linear soft actuators struggle to simultaneously generate high force and extension (*35*–*40*). Our optimized linear soft actuator design addresses this problem by generating the forces and extensions required for injection while also enabling large affordances to envelop leaves in a variety of poses. This advancement leads to more precise and repeatable injections, improving observations and helping find the best conditions for biological, environmental, and mechanical effects. As an end effector, the leaf gripper bridges contact-based and in vivo phenotyping, enabling high-throughput operations and advancements in plant bioengineering for precision agriculture.

RESULTS

Design criteria for the leaf gripper

The mechanisms of leaves to resist infiltration (Fig. 1B) and the limitations of current methods in overcoming these resistances (fig. S2)

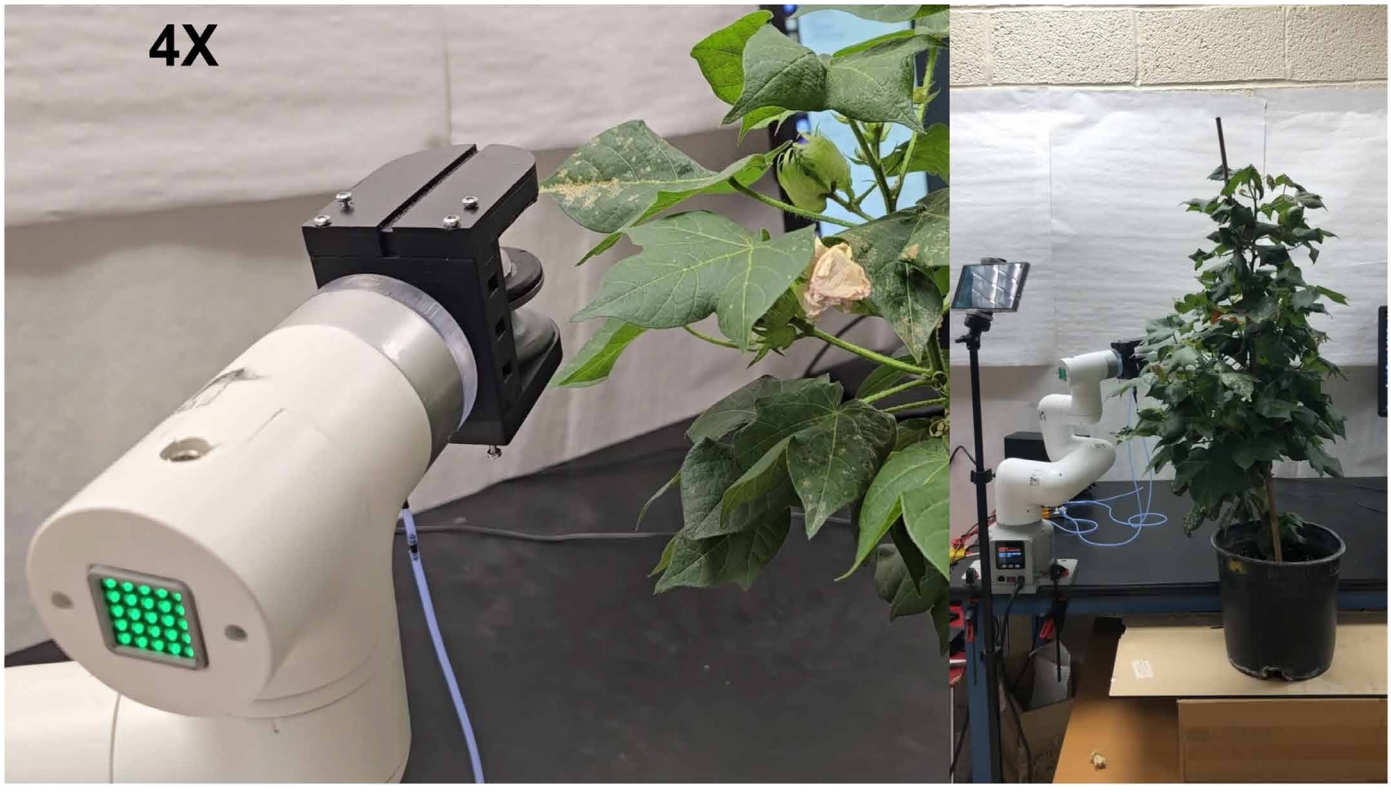

Movie 1. Research motivation and summary of methods and results.

motivated the development of a more effective injection technique. The ineffective results of spontaneous infiltration (fig. S2B) indicated that the ideal method should exert a large force. The use of vacuum chambers (fig. S2A) showed that this method of inducing pressure differentials was not an ideal solution for a portable system, because it increased the required volume of injectables by forcing the leaf to be submerged. Unfortunately, a more practical method having a vacuum on one side and liquid on the other side of the leaf was not a solution, because many plant species only have stomata on the abaxial (lower) side of their leaves (*41*). Although the syringe method has shown promising results for pressurized infiltration, it was not effective for heterobaric leaves (fig. S1) and was prone to causing leaf damage (fig. S2C). Our method met the criteria outlined in Fig. 1C as follows: First, it enhanced pressurized infiltration using a soft interface that included a gasket and sponge to stamp on the leaf, avoiding contact with rigid materials such as syringe tips and thus notably reducing leaf injury. Next, by increasing the contact area of the injection with a 20-mm-diameter sponge, which is almost an order of magnitude greater than the 3-mm outer diameter of a 1-ml needle-free syringe (26 gauge), the method overcame the compartmentation in heterobaric leaves by infiltrating many areoles in parallel, eliminating the need for spreading to reach those that are not in direct contact. Furthermore, the leaf gripper was portable because of its compact architecture, including a mini solenoid valve and mini pumps that could operate untethered with batteries (fig. S7). In addition, combining leaf grasping with foliar delivery made the stamping-injection method suitable for automation, whereas the viscoelastic nature of the soft actuator allowed for gentle stamping, making the method safer without the need for speed control. Overall, the combination of safe and effective leaf grasping, foliar delivery capabilities, and automation made the leaf gripper reliable and repeatable.

Component roles in the leaf gripper design

Figure 2A explains the roles and purposes of each component in addressing the various challenges that can arise during leaf grasping and injection. First, unstressed plant leaves were typically angled or tilted rather than flat, and their orientation could change throughout the day based on the Sun's position, as observed in cotton and sunflower plants (*42*, *43*). Robotic studies for leaf probing also needed to take leaf orientation into account during operations (*12*). The nonflat state of a leaf could cause spillage of the injectable at the leaf gripper during positioning. To address this issue, we used a commercial facial sponge in which we loaded the fluid before injection; this sponge prevented spillage at angles up to ±45° because of its porous structure and capillary action. These properties allowed the leaf gripper to adjust to the leaf's orientation. Trapped air on a submerged leaf surface (eq. S5 in Supplementary Materials and Methods) was also an issue given that it increased the surface tension, thereby reducing or preventing the infiltration (*44*); however, the sponge minimized trapped air by wetting the leaf surface just before stamping. Another issue was the leaf venation, which caused it to be rougher than expected; for example, a sunflower leaf's average thickness is 2.25 mm, whereas the midvein average thickness is 1.65 mm, and for cotton, the subvein, lateral vein, and midvein average thicknesses are 0.28, 0.85, and 1.40 mm (*45*, *46*). A gasket made of a hydrophobic soft material (Ecoflex 00-10, Smooth-On Inc.) provided effective sealing by adapting to varying vein thicknesses (t_{vein}), and the gasket displacement (Δx_{seal}) could reach up to 1.7 mm under an

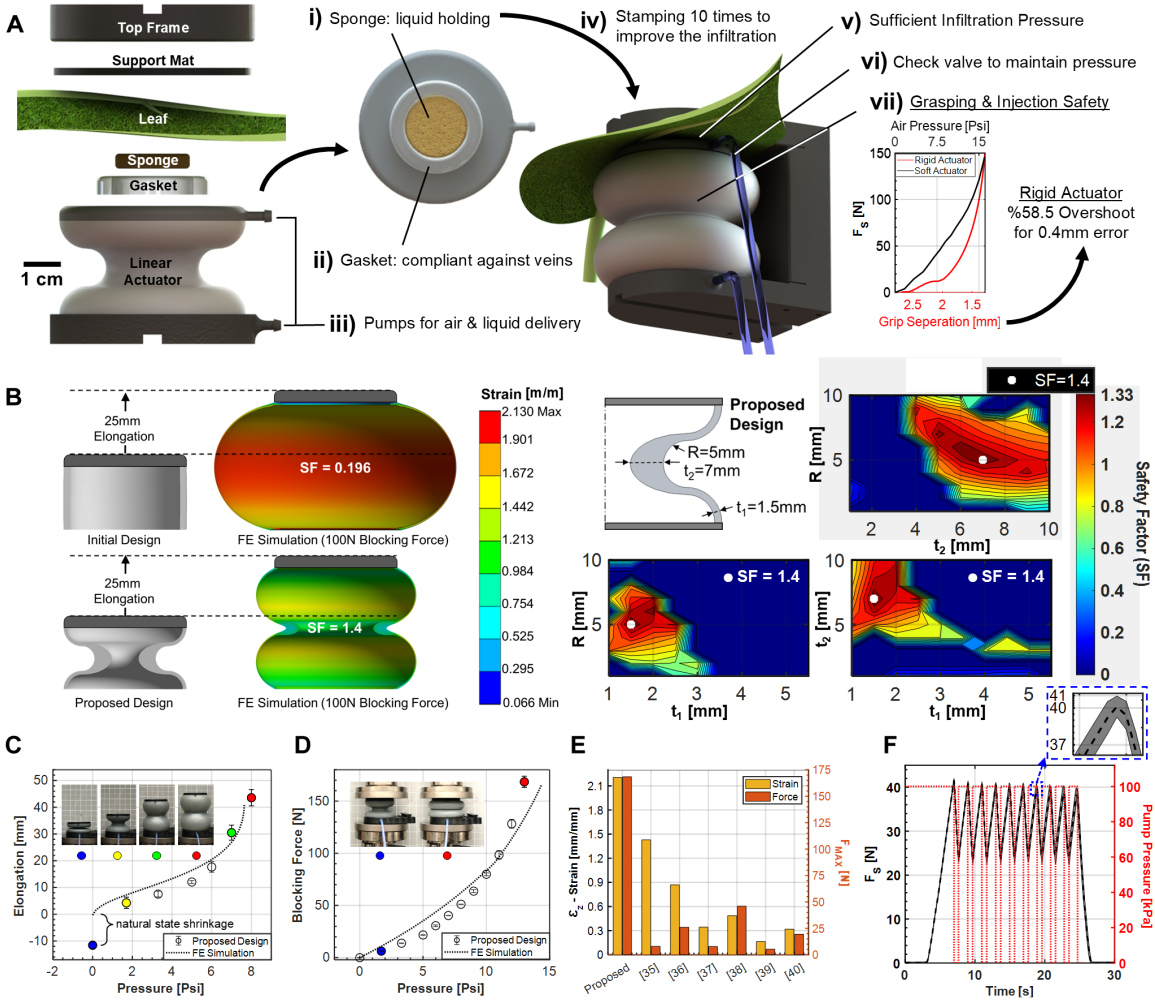

Fig. 2. Characterization of the leaf gripper. (**A**) Design choices for the sponge and gasket components and comparison of the soft actuator with its rigid counterpart. Scale bar, 1 cm. (**B**) Comparison of the initial flat design and the optimized design during extension with a 100-N contact force. The initial design demonstrates excessive radial displacement and an SF well below 1, indicating inadequate performance. In contrast, the optimized design achieves a safety factor of 1.4, substantially reducing radial displacement. Cross-sectional drawing with dimensions displays three input parameters for the parametric design, highlighting the optimized values. The remaining three contour plots depict the relationship between the input parameters and the SF for designs performing a 100-N output and 25-mm elongation. (**C**) Free elongation behavior based on air pressure. Data are presented as mean ± SD, with $n = 3$ biological replicates. (**D**) Fixed blocking force behavior based on air pressure. Data are presented as mean ± SD, with $n = 3$ biological replicates. (**E**) Performance comparison with other linear soft actuators in the literature (*35*–*40*). (**F**) Force profile during stamping injection. Each data point from the characterization tests consists of replicates from three different actuators. The dashed line represents the mean contact force, and the shaded gray region indicates ±1 SD.

applied stamping force ($\mathbf{F}_S$) as shown in eq. S7 in Supplementary Materials and Methods. In eq. S1, $\mathbf{F}_S$ was represented as $\mathbf{F}_{injection}$. In addition, the top frame was equipped with a thin layer of neoprene fabric to enhance the seal. This layer was stiffer than the gasket to prevent excessive deformation that could cause shear forces that mechanically damage the leaf (eq. S8). Stamping was the sole source of sealing and infiltration pressure, so the liquid pump only delivered media to the sponge before stamping. This limit was set because additional liquid pressure from the pump could have compromised the seal, causing the injectable to squirt out. This leakage is undesirable because it wastes cargo and compromises the precision of delivery to specific tissues. In addition, a check valve prevented injectables from flowing back into the pump during stamping. The soft actuator was a key component of the leaf gripper, given that it gently handled leaf grasping, sealing, and infiltration pressure because of its linear input-output relationship. Our design of this actuator was informed by the characterization of mechanical testing with a rigid actuator (ZwickRoell, Ulm, Germany); this testing illustrated that rigid interfaces were not ideal for leaf stamping because of the highly nonlinear relationship between force and distance, where a 0.4-mm error could result in a 58.5% overshoot. Further, force feedback control led to overshoots during injections because of the difficulty in measuring the soft interface presented by leaf tissue (fig. S14).

Design optimization for the actuator

The leaf gripper required a linear actuator because the stamping-injection method used only the normal force component. However, among various motion options, hydraulic actuators were better suited for bending and radial elongation rather than purely linear elongation, given that it was easier to inflate them in multiple directions

rather than solely along the axial direction (*47*). In addition, the leaf gripper design included a 25-mm gap for the actuator stroke during leaf grasping, which simplified the positioning of irregularly shaped leaves before injection. The actuator length matched this gap to maintain compactness. This configuration was challenging for the actuator, because it had to begin exerting force only after expanding to twice its original size. A systematic approach to designing soft actuators needed to incorporate simulation and optimization tools, given that each application required a unique design to meet specific criteria (*48*). To benefit from the design optimization, we applied screening-based optimization (Fig. 2B and fig. S4) using finite element analysis (fig. S3) and a parametric design study (fig. S5). The selected hourglass-shaped design featured smooth curvatures that reduced stress accumulation by eliminating sharp edges; this geometry also allowed us to use a small number of input parameters to modify the entire design. Although the design consisted of 11 total parameters, we focused on three key inputs: t_1, t_2, and R (shoulder thickness, waist thickness, and waist radius). The remaining parameters were either fixed (such as total length and diameter) or defined as functions of the input parameters (fig. S5). To evaluate each design for consistent performance, we used a custom Python script to scan pressure points from 0 to 100 kPa, identifying the pressure required to achieve a 25-mm elongation and a 100-N output force (fig. S4). We established the following boundary conditions for the input parameters: $1 < t_1$ (in millimeters) < 5.5, $1 < t_2$ (in millimeters) < 10, and $1 < R$ (in millimeters) < 10, with constraints R_5 (shoulder radius) ≥ 1 mm, $\mathbf{F}_B$ (blocking force) $= 100$ N, and $0 < P$ (in kilopascals) < 100. The output objective was to maximize the safety factor (SF = $S_{failure}/S_{max}$), where S_{max} (in megapascals) is the maximum stress applied during the application and $S_{failure}$ (in megapascals) is the stress at which structural failure occurs ($S_{failure} = 3.5$ MPa; SIL 30, Carbon). Consequently, from a total of 1000 designs, the optimized design parameters selected were $t_1 = 1.5$ mm, $t_2 = 7$ mm, and $R = 5$ mm, resulting in an SF = 1.4 and a radial displacement (δ_R) = 13.7 mm. In comparison, the results for our initial flat design were SF = 0.196 and $\delta_R = 26.3$ mm (Fig. 2B).

Characterization of the actuator

After optimizing the design, Fig. 2 (C and D) presents the characterization of the actuator with a free elongation test (Fig. 2C) and a blocking force test (Fig. 2D) on three different actuators with the same design. The free elongation test demonstrated that at $\Delta P = 55.2$ kPa (8 psi), the soft actuator elongated by 43.55 ± 3.1 mm; given the natural state displacement of 11.56 ± 1.1 mm in its unactuated state after curing, the total elongation was 55.12 ± 4.2 mm. The blocking force test demonstrated that when the actuator was fixed, it produced a force of 168.47 ± 5.34 N at $\Delta P = 89.6$ kPa (13 psi). The proposed design outperformed other linear soft actuators (*35*–*40*) in terms of both force and elongation (Fig. 2E and table S1). Figure 2F shows that the force profile during stamping for the actuator calibrated to 40 N, with the $\mathbf{F}_S$ peak reaching 40.54 ± 0.82 N, corresponding to the on-off time control of the air pump. In addition, the fatigue test showed that the actuator reliably completed more than 3700 stampings throughout its lifetime, with the $\mathbf{F}_S$ peak reaching 41.18 ± 1.29 N (fig. S8).

Evaluation of foliar delivery performance

Although infiltration resistance mechanisms directly influence plant water uptake (*24*, *41*, *44*, *49*), other environmental factors also create dynamic effects, such as influencing stomatal aperture, a (*50*). Current devices lack reliability and repeatability, preventing a distinct demonstration of these effects on the performance of an injection device (*28*). After the development of the leaf gripper with the stamping-injection method, we conducted tests on the leaves of two heterobaric species, sunflower and cotton, to characterize infiltration. The portable feature of the leaf gripper allowed in situ foliar delivery, ensuring that the plants remained in their original environments during infiltration. To investigate the effects of the state of the plants on the infiltration performance of the leaf gripper, we used three different growing conditions at Cornell University: GC1 (growth chamber; Guterman Bioclimatic Laboratory), GC2 (greenhouse; Guterman Bioclimatic Laboratory), and GC3 (growth chamber; Weill Hall Laboratory) (fig. S10). Figure 3A shows the measured parameters of growing conditions and sunflower stomatal conductance, again referred to as g_s, grown in the corresponding environments. Cotton plants are available for foliar delivery between the second and fifth months, whereas sunflower plants are available for a shorter period, between the 8th and 10th weeks, because of their rapid growth (fig. S10). The evaluation of infiltration performance relied on image processing of injection site pictures taken immediately after the injection to calculate the infiltration area and later to calculate the injured area (fig. S11). A portable LI-COR 600 porometer (LI-COR, Lincoln, NE, USA) enabled the measurement of humidity and temperature for leaf and environment, light, and stomatal conductance to water vapor, g_s (in moles per square meter per second) during each foliar delivery application; stomatal conductance was a monotonic increasing function of the aperture. Using these calculation techniques, Fig. 3B compares the effects of growing conditions, the syringe method, and different $\mathbf{F}_S$ values for the proposed method. Exceeding an upper limit of $\mathbf{F}_S$ increased the injured area (7 days after injections), and the noninjured infiltrated area [effective area (A_{EFF})] for different forces showed no notable change across different environments. For instance, A_{EFF} for $\mathbf{F}_S = 40$, 60, and 80 N was 2.14, 2.70, and 2.52 cm^2, respectively. Similarly, for cotton plants in GC2, A_{EFF} values were 5.75, 4.85, and 6.02 cm^2 (Fig. 3E). The figure also shows the relationship between infiltrated areas using the proposed method and g_s. The average infiltrated areas in GC1, GC2, and GC3 were 1.53, 4.31, and 3.84 cm^2, respectively, corresponding to g_s values of 0.077, 0.195, and 0.171 mol m^{-2} s^{-1}. To clarify the relationship, Fig. 3C shows that A_{EFF} and g_s had a correlation coefficient of 0.68, the highest among all factors. In addition, the second-highest correlation, with a coefficient of 0.63, was between A_{EFF} and relative humidity in the growing environment; this correlation likely relates to the influence of leaf humidity on g_s. Another factor affecting g_s is light, which accounts for the variation observed in GC2 (Fig. 3A). By injecting a cotton plant in the same environment throughout the day, we observed a noticeable increase in the infiltrated area around noontime (1:13 p.m.; 19 March 2024) as shown in Fig. 3D, whereas the area decreased when daylight decreased. The comparison between GC1 and other growing conditions provided key insights into which conditions to avoid for maintaining infiltration success, such as low humidity (17.9%), low g_s (0.077 mol m^{-2} s^{-1}), and low ambient light. For the rest of the study, we aimed to eliminate these unfavorable conditions by increasing irrigation when humidity was low and by performing infiltration around noon if sunlight was the primary light source, as in the greenhouse (GC2).

Evaluation across multiple species

In addition to the evaluations conducted with cotton and sunflower, as shown in fig. S13, the leaf gripper also achieved successful injections

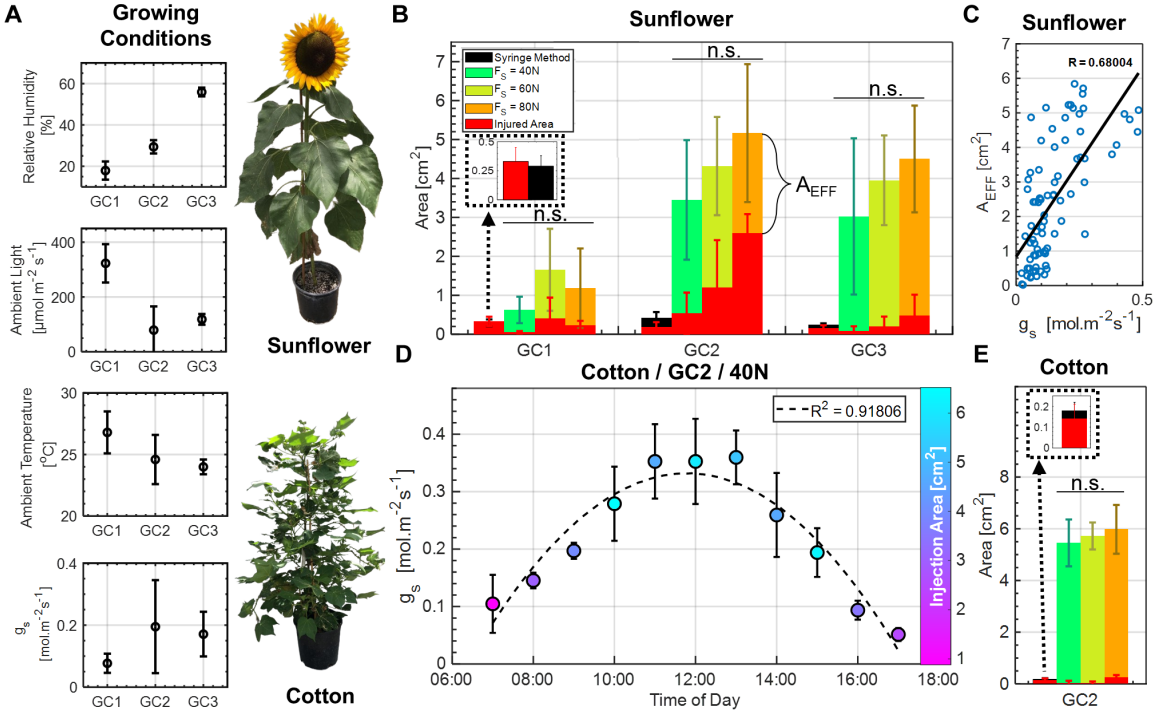

Fig. 3. Characterization of foliar delivery. (**A**) Comparison of three growing conditions (GC1, GC2, and GC3), each with three sunflower plants, on the basis of relative humidity, ambient light, temperature, and g_s. GC1 has the lowest g_s and humidity ranges. GC2, a greenhouse environment, shows the largest variation in g_s compared with the growth chambers in GC1 and GC3. Data are presented as mean ± SD, with $n = 27$ biological replicates. (**B**) Infiltrated and injured areas of sunflower plants using syringe injections compared with proposed method injections at $\mathbf{F}_S$ = 40, 60, and 80 N. Data are presented as mean ± SD, with $n = 9$ biological replicates. Bars labeled with "n.s." indicate no statistically significant differences between groups except the syringe method ($P > 0.05$, ANOVA with Tukey's test). A_{EFF}, or noninjured infiltrated area, does not increase with higher A_{EFF}. (**C**) After analyzing the correlation between A_{EFF} and various factors such as humidity, light, $\mathbf{F}_S$, and temperature, g_s was found to have the highest correlation coefficient ($r = 0.68$) with A_{EFF}, on the basis of 81 injections. (**D**) Analyzing further the behavior of the injected area and g_s regarding the time of day for cotton plants in GC2 with $\mathbf{F}_S = 40$ N. Data are presented as mean ± SD, with $n = 3$ biological replicates. (**E**) The proposed method once again shows no notable relationship between A_{EFF} and increased $\mathbf{F}_S$ for cotton plants. Data are presented as mean ± SD, with $n = 4$ biological replicates. Bars labeled with different letters (n.s.) indicate no statistically significant differences between groups except the syringe method ($P > 0.05$, ANOVA with Tukey's test).

in broad beans (*Vicia faba* L.), with lower heterobaricity, and milkweed (*Asclepias syriaca* L.), with medium heterobaricity. To address potential challenges with smaller leaves, we included images of infiltrated tomato seedlings, where the leaf size was smaller than our gripper's gasket. In this case, the entire leaf was infiltrated because the sealing effect formed a pressurized cuvette (fig. S13D). Outdoor applications further demonstrated that it is possible to inject a variety of plant types, provided that there are sufficient g_s values and thus stomatal openings or apertures (fig. S13E).

Nondamaging foliar delivery

We selected an $\mathbf{F}_S$ value of 40 N to minimize damage while ensuring sufficient injection at $P_{injection} = 48.3$ kPa (7 psi) (eq. S1). However, because of the selected interface elements, immediate leaf injury from tearing caused by shear forces did not occur until $P_{injection}$ reached 158.6 kPa (23 psi) ($P_{failure}$). In applying the SF concept to the leaf, we defined the SF of injection as $SF_{injection} = P_{failure}/P_{injection}$, which resulted in $SF_{injection} = 3.29$ for our application. Whereas infiltrated leaf areas turned darker green in the short term, injured areas became pale over time. On the basis of this observation, we assessed surface damage progression by capturing images of infiltrated areas after 7 days, manually marking regions that changed color, and calculating the injured area after image filtering, as shown in fig. S12. We also repeated this for the syringe injection; however, in some of the cases, tearing resulted in holes instead of a color change. The characterization of infiltration presented in Fig. 3 also demonstrates how the proposed method outperformed the traditional needle-free syringe method, even in challenging environments such as GC1. The average A_{EFF} for sunflowers under each growing condition was −0.04 (the injured area was larger than the injected area), 0.22, and 0.07 cm^2 (Fig. 3B), following the same order as that of g_s for the growth chambers, indicating a similar effect as seen with the proposed method. In addition, the average A_{EFF} for the syringe method on cotton in GC2 was 0.04 cm^2 (Fig. 3E). After determining the ideal conditions for infiltration, fig. S9 shows the success rate of the proposed method as 91.43% for 35 consecutive injections of sunflower in GC3. When compared with nonideal conditions in the same environment (Fig. 3B), the average g_s increased from 0.168 to 0.265 mol m^{-2} s^{-1}, whereas the average area of injection increased from 3.03 to 4.21 cm^2 and the average percentage of injured area decreased from 5.77 to 3.60%. In comparison, the syringe method resulted in an injured area percentage of up to 113.8% (Fig. 3B). Stomatal function after injection, as measured by g_s, can also serve as an indicator of the health of the injected leaf area because constant gas exchange levels correlated to stable biological functions. Figure S12 (A and B) portrayed the change in g_s before

and after the injections for cotton plants in GC1 and sunflower plants in GC2. Whereas the average g_s for sunflowers decreased substantially throughout 10 days with the syringe method (from 0.484 to 0.170 mol m^{-2} s^{-1}), the proposed method maintained a more stable behavior (from 0.471 to 0.441 mol m^{-2} s^{-1}). A similar trend was observed for cotton (syringe method: 0.385 to 0.049 mol m^{-2} s^{-1}; our method: 0.391 to 0.272 mol m^{-2} s^{-1}). The damage after injection falls into two categories: instant damage, where the leaf showed immediate cuts, and partial damage, which developed gradually as surface damage over time. With the proposed method, cotton showed no visible damage for the following 10 days (fig. S12C). In sunflowers, partial surface damage usually appeared after a week, with little to no damage during the first week (fig. S12D). The syringe method, however, frequently cut the leaves and caused instant damage (fig. S12C). For the longest observation period in this study, the injected leaves shown in Fig. 5D continued to grow normally for 56 days after treatment, until they were harvested for a destructive RNA analysis.

Nanoparticle delivery with the leaf gripper

For the initial in vivo phenotyping application with the leaf gripper, we used nanoparticles of hydrogel, called AquaDust in prior literature (*21*), that fluoresce proportionately to available water. The current foliar delivery method with syringes compromised the nondestructive nature of AquaDust by frequently cutting the leaf and may also have affected measurement accuracy. In addition, when the heterobaricity in the plant increased substantially, the A_{EFF} available for measurement could become too small, potentially rendering the method ineffective. Using the leaf gripper for foliar delivery of AquaDust reduced these risks and expanded its usability by remaining effective even in heterobaric leaves. To evaluate the effectiveness of the leaf gripper, we submerged the sponge with the AquaDust hydrogel nanoreporter solution (Fig. 4A) and infiltrated ~0.33 ml per injection into cotton leaves using our stamping method. Applying ideal conditions in GC1, as described in the previous section, helped plants to reach a higher g_s (an average of 0.411 mol m^{-2} s^{-1}) and sufficient infiltration area (an average of 4.82 cm^2). This process allowed us to study the response of outside-xylem zone (OXZ) apoplasmic water potentials (megapascals) to progressive drought (*21*). Our first test aimed to ensure that the leaves remained healthy after injection by verifying that AquaDust remained localized at the cell wall–air space interface of the mesophyll, bundle sheath, and epidermal tissue, without entering the cells and compromising measurements. Confocal micrographs (Fig. 4B) confirmed that the signal predominantly originated from AquaDust nanoparticles at the cell walls, although some nanoparticles did enter mesophyll and epidermal cells. We next examined the response of hydraulic conductance in the OXZ (g_{oxz}) to progressive drought because it provided insights into the passive regulation of transpiration. Although this response had been previously characterized in maize and tomato (*51*), we adapted this analysis to cotton using the leaf gripper (Fig. 4D), making it possible to study a plant type previously unsuitable for such analysis because of limitations in foliar delivery techniques. Figure 4C illustrates the normalized fluorescence intensity spectra from a region infiltrated with AquaDust; the calibrated signal of water potential was based on the relative height of the peaks associated with the donor and acceptor dyes. By combining AquaDust with porometer data, one can assess the hydraulic properties of the leaf. After the AquaDust injection, we measured leaf gas exchange parameters with a LI-COR 600 porometer, the apoplasmic water potential (ψ_i), and the local leaf xylem water potential (ψ_{xylem}) using an optical fiber probe (*21*, *51*) to evaluate g_{oxz}. The response of g_{oxz} to progressive drought, as characterized by local leaf xylem water potential [ψ_{xylem} (in megapascals)], is shown in Fig. 4D. If the water potential signal had primarily originated from AquaDust nanoparticles inside the mesophyll and epidermal cells, then the measurements would have consistently indicated values near saturation, given that AquaDust responded to the pressure potential and not the osmotic potential. These measurements confirmed that cell structures remained unharmed after the injections.

Gene delivery with the leaf gripper

For the second in vivo application using the leaf gripper, we evaluated *A. tumefaciens* infiltration ("agroinfiltration") to edit the leaf's DNA with the *RUBY* reporter system, which consisted of three genes that, respectively, encoded a P450 oxygenase (*CYP76AD1*), L–3,4-dihydroxyphenylalanine 4,5-dioxygenase (*DODA*), and a glucosyltransferase (*GT*) (*20*). The leaf converted tyrosine into vividly red betalain through three enzymatic reactions, resulting in a color change in the infiltrated area (Fig. 5A). This transformation provided a straightforward visual check of gene expression in various plant species, which was particularly valuable as gene editing became more widely used in fundamental plant research and crop improvement. It was also applicable in RNA silencing studies when inducers and suppressors were designed for manipulating the expression of *RUBY* genes (*52*). Conventional delivery methods, however, could have detrimental effects on plant tissues during application, an issue that the leaf gripper can help mitigate. Beyond the benefits mentioned before, the leaf gripper's gentle stamping approach also prevented the accidental dispersal of genetic material, reducing contamination risks common with syringe-based agroinfiltration. To demonstrate this benefit, we agroinfiltrated sunflower leaves after transferring a binary vector (pHDE-CaMV35Sp::*RUBY*::tHSP18.2) into an *A. tumefaciens* strain EHA105. Figure 5B presents a nondestructive analysis of betalain accumulation in the same infiltrated area in a time course. The remaining figures (Fig. 5, C to D) include nondestructive analyses using spectrophotometry to quantify betalain abundance and RT-qPCR (quantitative reverse transcription polymerase chain reaction) to evaluate the expression of *DODA*, a *RUBY* gene. We modeled the relationship between *DODA* expression and betalain accumulation over time, by analyzing the leaf coloration at different time points after agroinfiltration [days postinfiltration (DPI)]. We divided the measured agroinfiltration behavior into four periods. At 0 DPI, the RNA level was minimal, whereas betalain was not yet detectable. Around 3 DPI, *DODA* expression levels peaked, and betalain biosynthesis became visible. At 1 week (7 DPI), RNA levels began to decrease, whereas betalain accumulation peaked. Last, at 2 months, *DODA* expression was extremely low, whereas the betalain-pigmented phenotype remained. In addition to sunflower, broad bean also showed a similar *DODA* expression trend, as illustrated in fig. S13C.

DISCUSSION

Here, we presented a method for designing, manufacturing, and testing a soft robotic leaf gripper with a foliar delivery system. After highlighting how hydrophobicity and heterobaricity pose substantial challenges for foliar uptake, we proposed soft components for actuation, fluid delivery, and sealing to address these challenges. Specifically, we performed design optimization of linear soft actuators to reduce radial expansion and increase the ability of

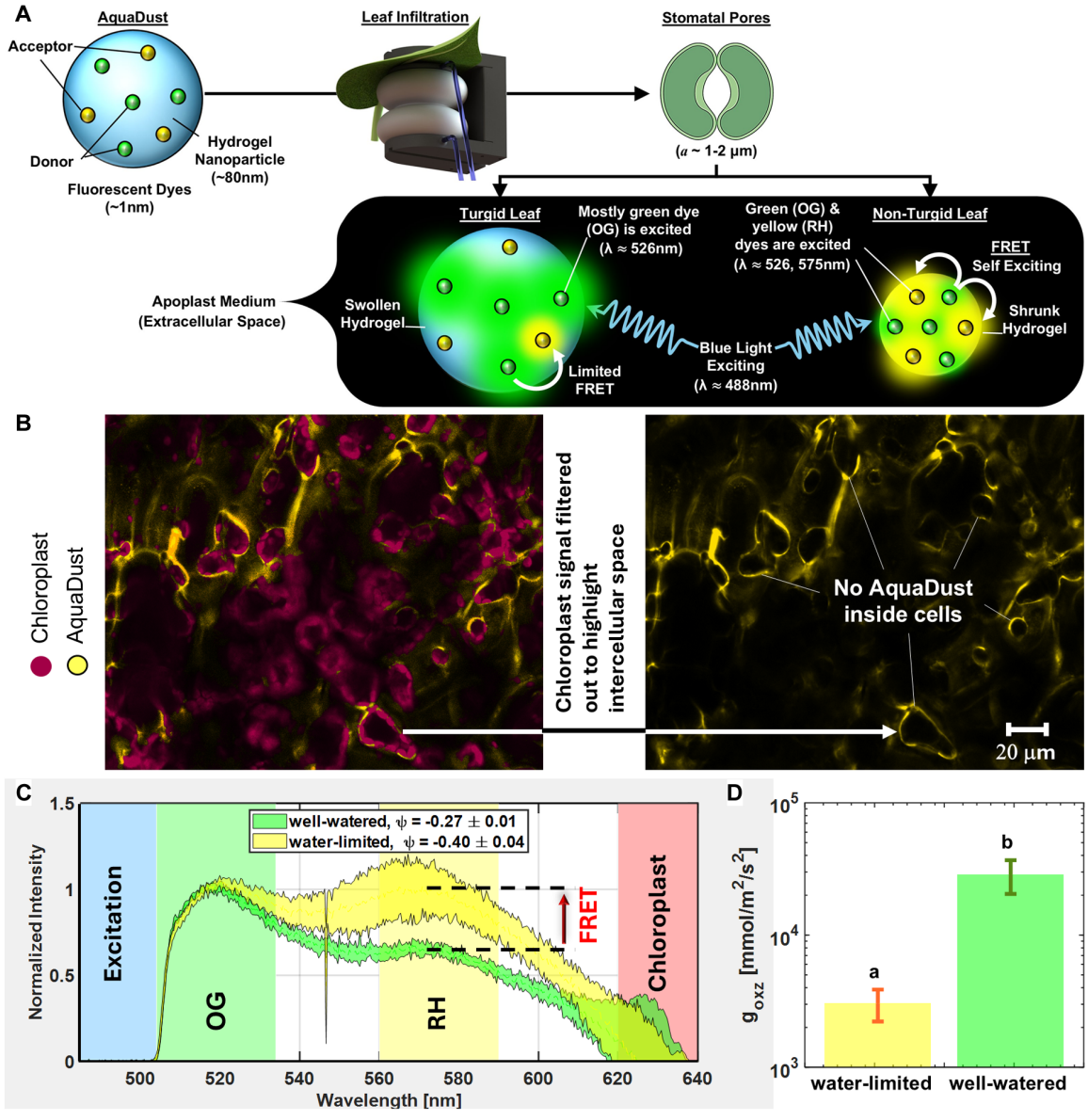

Fig. 4. AquaDust application for nanoparticle delivery with the leaf gripper. (**A**) The simplified mechanism for AquaDust shows its functions as a nanosensor to measure plant and environmental water stress upon injection. (**B**) Confocal microscopy images of injected AquaDust show red fluorescence from chloroplasts, which is used to locate the cells, whereas yellow fluorescence represents the acceptor dye (RH) of AquaDust. The dark regions after filtering out chloroplast fluorescence indicate that AquaDust primarily accumulated on the cell membranes with no substantial presence inside the cells, suggesting that the cell walls remained unharmed during injection. Scale bar, 20 µm. (**C**) Normalized fluorescence intensity spectra of a plant used in AquaDust sensing, showing wet and dry signals. The spectra show exciting, OG (donor), RH (acceptor), and chloroplast regions. The RH peak increased, reflecting higher FRET activity as the plant dried. (**D**) The relation between g_{oxz} and water status to model the transpiration behavior of the plant (*51*). Data are presented as mean ± SD, with $n = 3$ biological replicates. Bars labeled with different letters (a and b) indicate statistically significant differences between groups ($P < 0.05$, ANOVA with Tukey's test).

force exertion. Moreover, we evaluated the effects of environmental, biological, and mechanical factors on probe injection and performance, proposing the ideal conditions for better infiltration. Next, we discussed the leaf safety provided by two key features: the soft interface for the leaf and the gentle stamping capability of the actuator, enabled by its viscoelastic properties. Furthermore, we integrated the leaf gripper onto a robot arm for injecting leaves to highlight its ease of implementation for automated field phenotyping. We used a learning-by-demonstration approach, specifically kinesthetic guiding, using the myCobot 280 M5Stack arm in gravity compensation mode, whereas the gripper performed autonomous injection. Last, we showcased primary foliar delivery applications: nanoparticle injection and genetic transformation, which allowed us to conduct three different levels of optical measurements—confocal microscopy, spectrometry, and naked-eye observation (table S2).

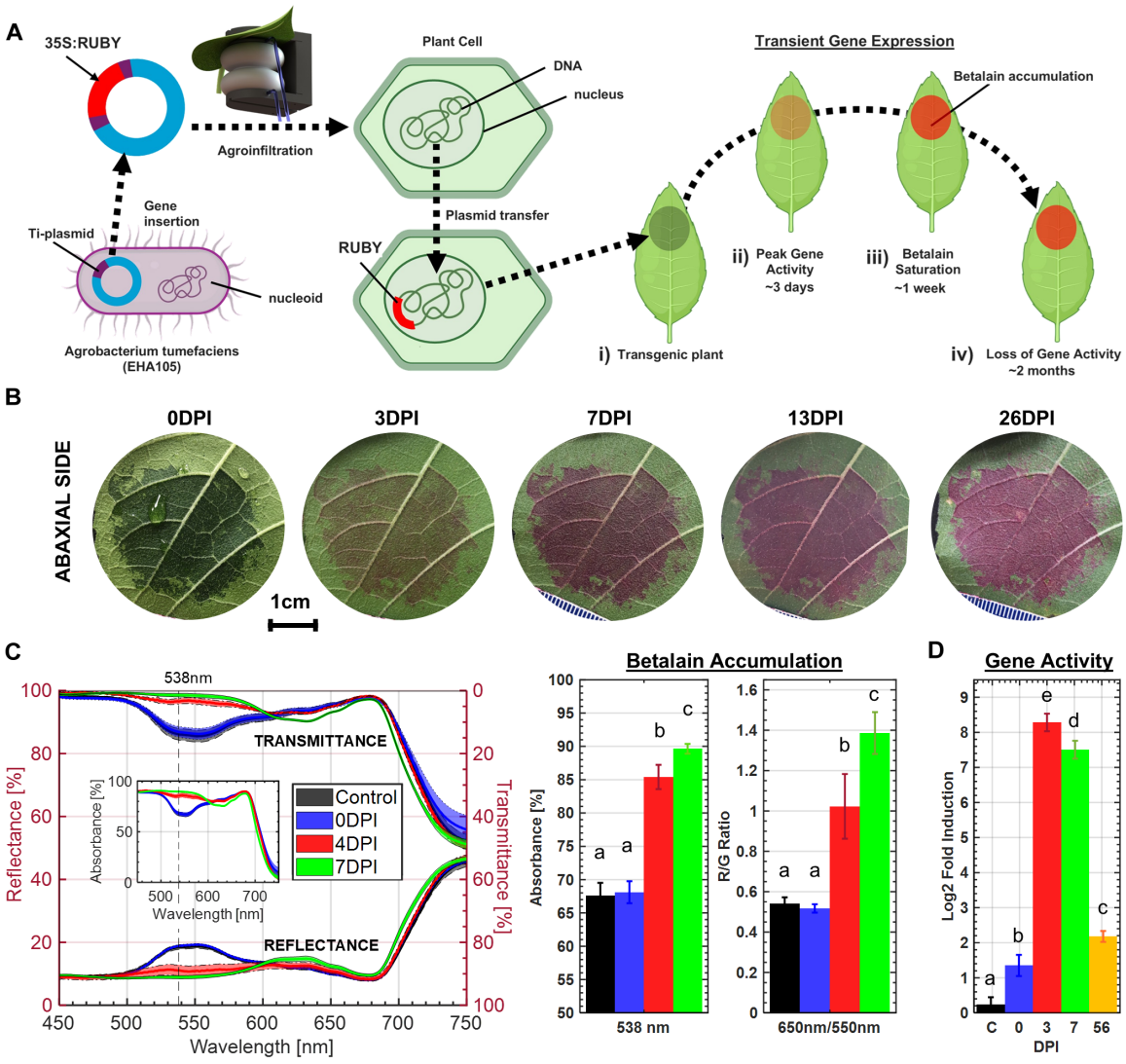

Fig. 5. Agroinfiltration application for gene delivery with the leaf gripper. (**A**) Simplified mechanism of agroinfiltration for transient gene expression in plants. The *RUBY* reporter system, encoding *CYP76AD1*, *DODA*, and a *GT*, generally shows transient activity for up to 8 weeks, whereas betalain accumulation, serving as a visual reporter, peaks within 1 week and remains visible in the plant. (**B**) Pictures of betalain accumulation in a sunflower plant over time. Scale bar, 1 cm. (**C**) Profiles of reflectance, transmittance, and absorbance spectra of agroinfiltrated sunflower leaves were measured over time in this study. Absorbance measurements at 538 nm for quantifying the betalain on the basis of the literature (*52*, *55*). The red-green ratio of leaf reflectance values corresponded to 650 and 550 nm on the basis of the literature (*56*). Data are presented as mean ± SD, with $n = 3$ biological replicates. Bars labeled with different letters (a, b, and c) indicate statistically significant differences between groups ($P < 0.05$, ANOVA with Tukey's test). (**D**) The expression of *DODA* in sunflower leaves after agroinfiltration. Data are presented as mean ± SD, with $n = 3$ biological replicates. Bars labeled with different letters (a, b, c, d, and e) indicate statistically significant differences between groups ($P < 0.05$, ANOVA with Tukey's test).

Generalizing the leaf gripper performance

The leaf gripper extends the range of foliar delivery applications beyond plants with low heterobaricity, as demonstrated with cotton and sunflower (fig. S1). Its applications are not limited to these two species, given that it has also shown successful results on plants with varying heterobaricity levels, such as broad bean and milkweed, and on plants of different sizes, including small tomato seedlings (fig. S13). In addition, it has the potential to be used on larger leaves, provided that $A_{\text{infiltration}}$ is sufficient or distributed information is not required. The proposed soft actuator design can also generate $\mathbf{F}_S$ values higher than 40 N, reaching up to 100 N (Fig. 2B), although this comes at the cost of a reduced life span.

As an automated foliar delivery device, the leaf gripper enhances plant bioengineering by providing controlled infiltrations. However, integrating it with robotic arms and rover technologies could further accelerate large-scale studies through automation, which is crucial for complex research, such as understanding genotype-phenotype relationships that require extensive analysis (*53*) or conducting field studies with large populations.

The leaf gripper also has a substantial potential for high-throughput phenotyping applications that can improve precision agriculture. Its in vivo applications with nanoparticles and genes already offer a wide range of indicators for accurately measuring various plant attributes. In addition, the gripper's gentle design makes it suitable for safe

contact-based phenotyping, such as leaf stiffness assessments that can be linked to ψ or gas exchange measurements, all without causing damage to the leaves.

MATERIALS AND METHODS

Measuring actuator contact force

We used the ZwickRoell Z010 material tensile testing machine to characterize the soft linear actuator by measuring the blocking force (Fig. 2D), calibrating and assessing the stamping-injection profile (Fig. 2F), and conducting fatigue tests (fig. S8). The device also served as a rigid alternative to the soft linear actuator and frequently showed overshooting because of sensitivity issues when measuring very soft objects (Fig. 2A, vii). In addition, we used it to calculate the pressure required for the soft interface to cause instant leaf injury.

Simulations

A finite element solver program (Ansys 2022) was used to optimize the design through iterative simulations, eliminating the need for physical prototypes. Initially, we characterized the hyperelastic properties of the elastic material (SIL 30, Carbon) using curve fitting based on uniaxial tensile test data (500 mm/min; American Society for Testing and Materials D412, Die C). We determined the third-order Yeoh model coefficients as C10 = 0.1675 MPa, C20 = 453.53 Pa, and C30 = 5.537 Pa, achieving a normalized residual sum of squares of 3.006. For blocking force simulations, we set the contact stiffness at 200 N/mm^3 to allow for faster convergence with sufficient accuracy, indicated by a maximum penetration of 1.389 μm. A two-dimensional (2D) axisymmetric simulation, using a 1-mm nonlinear quadratic mesh element size with an average skewness of 0.104, finished in about 25 s.

Fabrication

After designing the leaf gripper, we used the Carbon M1 DLS 3D printer for the precise and rapid manufacturing of the soft actuator (fig. S6B). We separately printed two main components using two different materials, namely, rigid (RPU 70, Carbon) and elastic (SIL 30, Carbon), and the components were easily assembled because of their ability to bond to each other during the thermal curing process. The printing process took ~5 hours, with a material cost of around $48 (table S3). To automate the stamping-injection process, we used a mini diaphragm pump for the air source, a solenoid valve for the soft actuator, a mini peristaltic pump for the liquid source, and an Arduino Uno microcontroller to control the process (fig. S7). The equipment cost was approximately $107, bringing the total cost of the leaf gripper to around $155 (table S4).

AquaDust

AquaDust occupied the space between plant cells (apoplast). It consisted of a hydrogel matrix containing both excited fluorescent particles (donors) and nonexcited fluorescent particles (acceptors). The donor particles were Oregon Green (OG) 488 *N*-hydroxy succinimidyl ester, and the acceptor particles were *N*-hydroxy succinimidyl ester rhodamine (RH). As the hydrogel shrunk because of dehydration, the distance between the donor and acceptor particles decreased, enhancing acceptor emission through Förster resonance energy transfer (FRET; Fig. 4A). This shift in the emission spectrum was gradual and allowed for precise, repeated, and nondestructive measurements of the plant's water potential (ψ) with units of megapascals; this method complemented the conventional, benchmark method based on the Scholander pressure chamber, which was destructive (given that it required cutting the leaf) and challenging (because of the need for high pressures, around 2 MPa). AquaDust-infiltrated regions allowed for measurements of ψ for up to 5 days, after which light caused the bleaching of the fluorescent dyes.

RNA analyses

We used a previously cloned *RUBY* gene cassette, which included the constitutive CaMV35S promoter (CaMV35Sp) and the HSP18.2 terminator (tHSP18.2) from *Arabidopsis* in the plasmid pHDE (*20*). The plasmid was transformed into *A. tumefaciens* strain EHA105, which was grown overnight in Luria-Bertani medium, resuspended in agroinfiltration buffer (10 mM MES at pH 5.8, 10 mM $MgCl_2$, and 200 μM acetosyringone) to a final optical density of 0.5, and then infiltrated into sunflower leaves using a leaf gripper. The agroinfiltrated areas were collected, flash-frozen in liquid nitrogen, and homogenized using the Geno Grinder 1600 MiniG (SPEX Sample Prep, USA). Total RNA was extracted from the samples using an RNA isolation kit (Promega Corp., USA) and subsequently reverse-transcribed with SMART MMLV reverse transcriptase (Takara Bio, Japan). For qPCR, each reaction mixture consisted of 5 μl of PowerUp SYBR Green PCR master mix (Applied Biosystems), 1 μl of each qPCR primer (table S5), and 1 μl of 10-fold diluted cDNA template. The PCR protocol consisted of an initial incubation at 95°C for 30 s, followed by 40 cycles of 95°C for 5 s and 60°C for 1 min, ending with a melting curve analysis. *ACT7* (*actin-7*) from *Helianthus annuus* served as the reference gene, and the relative expression levels of *DODA* (a *RUBY* gene) were determined using the method previously described (*54*).

Optical measurements

Fluorescence microscopy

We visualized AquaDust-infiltrated cotton leaves via a Zeiss LSM 880 confocal upright microscope (Fig. 4B). The leaves were mounted on a glass slide with double-sided tape and imaged using a W Plan-Apochromat 20×/1.0 water immersion objective. We also excited the two different fluorescent dyes in AquaDust separately: 500 nm for OG and 575 nm for RH.

Spectrometer

We used an Ocean Optics ST2000 spectrometer for measuring FRET between two dyes after exciting only the acceptor dye from AquaDust (Fig. 4C) by a mercury lamp light source (Leica EL6000) with a narrow-band optical filter (470 to 500 nm). After excitation, a reflection probe (QR600-7-UV-125F, Premium 600-μm reflection probe, Ocean Optics Inc.) was used to measure the reflected light, and the OceanView software was used to record the collected fluorescence intensity from both acceptor and donor dyes.

Spectrophotometer

We quantified the color change of agroinfiltrated cotton leaves via the Agilent Cary 5000 ultraviolet–visible–near infrared spectrophotometer by measuring transmission and reflectance over a wavelength range of 350 to 800 nm using an internal diffuse reflectance accessory consisting of a 25-mm-diameter integrating sphere.

Naked-eye observation

We tracked visible color changes due to betalain accumulation by naked-eye observation in agroinfiltrated cotton plants (Fig. 5B). This approach also facilitated the calculation of infiltrated and injured areas on the leaf throughout the study (Figs. 3 to 5 and fig. S9) via the method in fig. S11.

Statistical analysis

We calculated mean values (± SD) for Fig. 3A (samples: $n = 27$ for each bar), Fig. 3B ($n = 9$ for each bar), Fig. 3D ($n = 3$ for each marker), Fig. 3E ($n = 4$ for each bar), and Fig. 3C (right-top and bottom; $n = 3$ for each bar). Next, we used MATLAB R2023a to generate linear and curve-fitting plots in Fig. 3 (C and D). Last, we performed data analysis on the datasets shown in Figs. 3 to 5 using analysis of variance (ANOVA) with a significance threshold of $P < 0.05$.

Supplementary Materials

The PDF file includes:
Materials and Methods
Figs. S1 to S14
Tables S1 to S5
References (*57*–*63*)

Other Supplementary Material for this manuscript includes the following:
Movies S1 and S2
MDAR Reproducibility Checklist

REFERENCES AND NOTES

1. R. Gebbers, V. I. Adamchuk, Precision agriculture and food security. *Science* **327**, 828–831 (2010).
2. A. McBratney, B. Whelan, T. Ancev, J. Bouma, Future directions of precision agriculture. *Precis. Agric.* **6**, 7–23 (2005).
3. N. Zhang, M. Wang, N. Wang, Precision agriculture—A worldwide overview. *Comput. Electron. Agric.* **36**, 113–132 (2002).
4. N. M. Abd El-Ghany, S. E. Abd El-Aziz, S. S. Marei, A review: Application of remote sensing as a promising strategy for insect pests and diseases management. *Environ. Sci. Pollut. Res.* **27**, 33503–33515 (2020).
5. J. Rasmussen, S. Azim, J. Nielsen, Pre-harvest weed mapping of *Cirsium arvense* L. based on free satellite imagery—The importance of weed aggregation and image resolution. *Eur. J. Agron.* **130**, 126373 (2021).
6. R. A. Schwalbert, T. Amado, G. Corassa, L. P. Pott, P. V. V. Prasad, I. A. Ciampitti, Satellite-based soybean yield forecast: Integrating machine learning and weather data for improving crop yield prediction in southern Brazil. *Agric. For. Meteorol.* **284**, 107886 (2020).
7. J. U. H. Eitel, D. S. Long, P. E. Gessler, A. M. S. Smith, Using in-situ measurements to evaluate the new RapidEye™ satellite series for prediction of wheat nitrogen status. *Int. J. Remote Sens.* **28**, 4183–4190 (2007).
8. X. Meng, Y. Bao, J. Liu, H. Liu, X. Zhang, Y. Zhang, P. Wang, H. Tang, F. Kong, Regional soil organic carbon prediction model based on a discrete wavelet analysis of hyperspectral satellite data. *Int. J. Appl. Earth Obs. Geoinf.* **89**, 102111 (2020).
9. N. Pettorelli, J. O. Vik, A. Mysterud, J.-M. Gaillard, C. J. Tucker, N. C. Stenseth, Using the satellite-derived NDVI to assess ecological responses to environmental change. *Trends Ecol. Evol.* **20**, 503–510 (2005).
10. G. Lee, Q. Wei, Y. Zhu, Emerging wearable sensors for plant health monitoring. *Adv. Funct. Mater.* **31**, 2106475 (2021).
11. Z. Li, Y. Liu, O. Hossain, R. Paul, S. Yao, S. Wu, J. B. Ristaino, Y. Zhu, Q. Wei, Real-time monitoring of plant stresses via chemiresistive profiling of leaf volatiles by a wearable sensor. *Matter* **4**, 2553–2570 (2021).
12. A. Atefi, Y. Ge, S. Pitla, J. Schnable, Robotic technologies for high-throughput plant phenotyping: Contemporary reviews and future perspectives. *Front. Plant Sci.* **12**, 611940 (2021).
13. H. Zhao, K. O'Brien, S. Li, R. F. Shepherd, Optoelectronically innervated soft prosthetic hand via stretchable optical waveguides. *Sci. Robot.* **1**, eaai7529 (2016).
14. M. Usman, M. Farooq, A. Wakeel, A. Nawaz, S. A. Cheema, H. ur Rehman, I. Ashraf, M. Sanaullah, Nanotechnology in agriculture: Current status, challenges and future opportunities. *Sci. Total Environ.* **721**, 137778 (2020).
15. J. P. Giraldo, M. P. Landry, S. M. Faltermeier, T. P. McNicholas, N. M. Iverson, A. A. Boghossian, N. F. Reuel, A. J. Hilmer, F. Sen, J. A. Brew, M. S. Strano, Plant nanobionics approach to augment photosynthesis and biochemical sensing. *Nat. Mater.* **13**, 400–408 (2014).
16. C. Kaya, M. Ashraf, Foliar fertilization: A potential strategy for improving plant salt tolerance. *Crit. Rev. Plant Sci.* **43**, 1–23 (2023).
17. M. R. Hanson, R. H. Köhler, GFP imaging: Methodology and application to investigate cellular compartmentation in plants. *J. Exp. Bot.* **52**, 529–539 (2001).
18. M. Toyota, D. Spencer, S. Sawai-Toyota, W. Jiaqi, T. Zhang, A. J. Koo, G. A. Howe, S. Gilroy, Glutamate triggers long-distance, calcium-based plant defense signaling. *Science* **361**, 1112–1115 (2018).
19. K. Leuzinger, M. Dent, J. Hurtado, J. Stahnke, H. Lai, X. Zhou, Q. Chen, Efficient agroinfiltration of plants for high-level transient expression of recombinant proteins. *J. Vis. Exp.* **77**, e50521 (2013).
20. Y. He, T. Zhang, H. Sun, H. Zhan, Y. Zhao, A reporter for noninvasively monitoring gene expression and plant transformation. *Hortic. Res.* **7**, 152 (2020).
21. P. Jain, W. Liu, S. Zhu, C. Y.-Y. Chang, J. Melkonian, F. E. Rockwell, D. Pauli, Y. Sun, W. R. Zipfel, N. M. Holbrook, S. J. Riha, M. A. Gore, A. D. Stroock, A minimally disruptive method for measuring water potential in planta using hydrogel nanoreporters. *Proc. Natl. Acad. Sci. U.S.A.* **118**, e2008276118 (2021).
22. M. H. Wong, J. P. Giraldo, S.-Y. Kwak, V. B. Koman, R. Sinclair, T. T. S. Lew, G. Bisker, P. Liu, M. S. Strano, Nitroaromatic detection and infrared communication from wild-type plants using plant nanobionics. *Nat. Mater.* **16**, 264–272 (2017).
23. M. Melotto, W. Underwood, J. Koczan, K. Nomura, S. Y. He, Plant stomata function in innate immunity against bacterial invasion. *Cell* **126**, 969–980 (2006).
24. B. H. P. Rosado, C. D. Holder, The significance of leaf water repellency in ecohydrological research: A review. *Ecohydrology* **6**, 150–161 (2013).
25. M. A. M. Barbosa, D. H. Chitwood, A. A. Azevedo, W. L. Araújo, D. M. Ribeiro, L. E. P. Peres, S. C. V. Martins, A. Zsögön, Bundle sheath extensions affect leaf structural and physiological plasticity in response to irradiance. *Plant Cell Environ.* **42**, 1575–1589 (2019).
26. T. Lawson, J. Morison, Visualising patterns of CO_2 diffusion in leaves. *New Phytol.* **169**, 641–643 (2006).
27. M. M. Chaves, J. M. Costa, N. J. Madeira Saibo, "Chapter 3—Recent advances in photosynthesis under drought and salinity," in *Advances in Botanical Research of Plant Responses to Drought and Salinity Stress*, I. Turkan, Ed. (Academic Press, 2011), vol. 57, pp. 49–104.
28. I. A. Chincinska, Leaf infiltration in plant science: Old method, new possibilities. *Plant Methods* **17**, 83 (2021).
29. Z. Zhou, C. Cao, L. Cao, L. Zheng, J. Xu, F. Li, Q. Huang, Effect of surfactant concentration on the evaporation of droplets on cotton (*Gossypium hirsutum* L.) leaves. *Colloids Surf. B Biointerfaces* **167**, 206–212 (2018).
30. P. L. Healey, R. Ernst, J. Arditti, Biological effects of surfactants. *New Phytol.* **70**, 477–482 (1971).
31. C. W. Simmons, J. S. VanderGheynst, S. K. Upadhyaya, A model of *Agrobacterium tumefaciens* vacuum infiltration into harvested leaf tissue and subsequent in planta transgene transient expression. *Biotechnol. Bioeng.* **102**, 965–970 (2009).
32. V. B. Koman, M. Park, T. T. S. Lew, S. Wan, E. S. Yarwood, X. Gong, T. S. Shikdar, R. J. Oliver, J. Cui, P. Gordiichuk, R. Sarojam, M. S. Strano, Emerging investigator series: Linking nanoparticle infiltration and stomatal dynamics for plant nanobionics. *Environ. Sci. Nano* **9**, 1236–1246 (2022).
33. N. R. Sinatra, C. B. Teeple, D. M. Vogt, K. K. Parker, D. F. Gruber, R. J. Wood, Ultragentle manipulation of delicate structures using a soft robotic gripper. *Sci. Robot.* **4**, eaax5425 (2019).
34. H. Yuk, S. Lin, C. Ma, M. Takaffoli, N. X. Fang, X. Zhao, Hydraulic hydrogel actuators and robots optically and sonically camouflaged in water. *Nat. Commun.* **8**, 14230 (2017).
35. P. Moseley, J. M. Florez, H. A. Sonar, G. Agarwal, W. Curtin, J. Paik, Modeling, design, and development of soft pneumatic actuators with finite element method. *Adv. Eng. Mater.* **18**, 978–988 (2016).
36. T. Kanno, S. Ohkura, O. Azami, T. Miyazaki, T. Kawase, K. Kawashima, Model of a coil-reinforced cylindrical soft actuator. *Appl. Sci.* **9**, 2109 (2019).
37. R. Hashem, M. Stommel, L. K. Cheng, W. Xu, Design and characterization of a bellows-driven soft pneumatic actuator. *IEEEASME Trans. Mechatron.* **26**, 2327–2338 (2021).
38. F. Chen, Y. Miao, L. Zhang, S. Chen, X. Zhu, Triply periodic channels enable soft pneumatic linear actuator with single material and scalability. *IEEE Robot. Autom. Lett.* **7**, 2668–2675 (2022).
39. Y. Zhu, K. Chu, X. Chen, X. Wang, H. Su, Research and application of a multi-degree-of-freedom soft actuator. *Sens. Actuators, Phys.* **338**, 113492 (2022).
40. R. Drury, V. Sencadas, G. Alici, 3D printed linear soft multi-mode actuators expanding robotic applications. *Soft Matter* **18**, 1911–1919 (2022).
41. Y. Su, V. Ashworth, C. Kim, A. S. Adeleye, P. Rolshausen, C. Roper, J. White, D. Jassby, Delivery, uptake, fate, and transport of engineered nanoparticles in plants: A critical review and data analysis. *Environ. Sci. Nano* **6**, 2311–2331 (2019).
42. A. R. G. Lang, Leaf orientation of a cotton plant. *Agric. Meteorol.* **11**, 37–51 (1973).
43. G. S. G. Shell, A. R. G. Lang, Movements of sunflower leaves over a 24-h period. *Agric. Meteorol.* **16**, 161–170 (1976).
44. C. W. Extrand, Repellency of the lotus leaf: Resistance to water intrusion under hydrostatic pressure. *Langmuir* **27**, 6920–6925 (2011).
45. D. S. Fensom, R. G. Donald, Thickness fluctuations in veins of corn and sunflower detected by a linear transducer. *J. Exp. Bot.* **33**, 1176–1184 (1982).
46. A. Sharma, R. Singh, Oviposition preference of cotton leafhopper in relation to leaf-vein morphology. *J. Appl. Entomol.* **126**, 538–544 (2002).
47. X. Tang, H. Li, T. Ma, Y. Yang, J. Luo, H. Wang, P. Jiang, A review of soft actuator motion: Actuation, design, manufacturing and applications. *Actuators* **11**, 331 (2022).

48. M. S. Xavier, C. D. Tawk, A. Zolfagharian, J. Pinskier, D. Howard, T. Young, J. Lai, S. M. Harrison, Y. K. Yong, M. Bodaghi, A. J. Fleming, Soft pneumatic actuators: A review of design, fabrication, modeling, sensing, control and applications. *IEEE Access* **10**, 59442–59485 (2022).
49. Y. He, S. Xiao, J. Wu, H. Fang, Influence of multiple factors on the wettability and surface free energy of leaf surface. *Appl. Sci.* **9**, 593 (2019).
50. T. N. Buckley, How do stomata respond to water status? *New Phytol.* **224**, 21–36 (2019).
51. P. Jain, A. E. Huber, F. E. Rockwell, S. Sen, N. M. Holbrook, A. D. Stroock, New approaches to dissect leaf hydraulics reveal large gradients in living tissues of tomato leaves. *New Phytol.* **242**, 453–465 (2024).
52. M. Tabara, A. Matsumoto, Y. Kibayashi, A. Takeda, K. Motomura, Straightforward and affordable agroinfiltration with RUBY accelerates RNA silencing research. *Plant Mol. Biol.* **114**, 61 (2024).
53. D. K. Großkinsky, J. Svensgaard, S. Christensen, T. Roitsch, Plant phenomics and the need for physiological phenotyping across scales to narrow the genotype-to-phenotype knowledge gap. *J. Exp. Bot.* **66**, 5429–5440 (2015).
54. K. J. Livak, T. D. Schmittgen, Analysis of relative gene expression data using real-time quantitative PCR and the $2^{-\Delta\Delta CT}$ method. *Methods* **25**, 402–408 (2001).
55. E. Tomizawa, S. Ohtomo, K. Asai, Y. Ohta, Y. Takiue, A. Hasumi, M. Nishihara, T. Nakatsuka, Additional betalain accumulation by genetic engineering leads to a novel flower color in lisianthus (*Eustoma grandiflorum*). *Plant Biotechnol.* **38**, 323–330 (2021).
56. A. Viña, A. A. Gitelson, Sensitivity to foliar anthocyanin content of vegetation indices using green reflectance. *IEEE Geosci. Remote Sens. Lett.* **8**, 464–468 (2011).
57. K. E. Fry, R. B. Walker, A pressure-infiltration method for estimating stomatal opening in conifers. *Ecology* **48**, 155–157 (1967).
58. N. K. Adam, *The Physics and Chemistry of Surfaces* (Oxford Univ. Press, 1941).
59. D. Ye, S. N. Kiemle, S. Rongpipi, X. Wang, C. Wang, D. J. Cosgrove, E. W. Gomez, E. D. Gomez, Resonant soft x-ray scattering reveals cellulose microfibril spacing in plant primary cell walls. *Sci. Rep.* **8**, 12449 (2018).
60. T. Lawson, W. James, J. Weyers, A surrogate measure of stomatal aperture. *J. Exp. Bot.* **49**, 1397–1403 (1998).
61. C. A. Brewer, W. K. Smith, T. C. Vogelmann, Functional interaction between leaf trichomes, leaf wettability and the optical properties of water droplets. *Plant Cell Environ.* **14**, 955–962 (1991).
62. D. R. Lee, Elasticity of phloem tissues1. *J. Exp. Bot.* **32**, 251–260 (1981).
63. A. Schiavi, A. Prato, "Elastic and viscoelastic properties of synthetic rubber (polychloroprene): Dynamic and static characterization," in *Proceedings of the 24th International Congress on Sound and Vibration* (Institute of Acoustics, 2017), pp. 1–8.

Acknowledgments

Funding: This work was supported by the TÜBİTAK-2219 project under grant no. 1059B192200535, the National Science Foundation under grant no. DBI-2019674, and the USDA National Institute of Food and Agriculture, contract no. 2021-67021-33843. **Author contributions:** Conceptualization: A.D.S. and R.F.S. Methodology: M.M.I., A.H., A.K.M., T.L., and A.D.S. Investigation: M.M.I., A.H., S.S., F.W., and T.L. Visualization: M.M.I., S.S., and F.W. Funding acquisition: A.D.S. and R.F.S. Project administration: A.D.S. and R.F.S. Supervision: G.J., A.D.S., and R.F.S. Writing—original draft: M.M.I. and F.W. Writing—review and editing: M.M.I., F.W., S.S., G.J., A.D.S., and R.F.S. **Competing interests:** The authors declare that they have no competing interests. **Data and materials availability:** All data and code needed to evaluate the conclusions in this paper are available in the paper, the Supplementary Materials, or the Dryad repository at DOI: 10.5061/dryad.9kd51c5vm.

Submitted 30 October 2024
Accepted 14 May 2025
Published 11 June 2025
10.1126/scirobotics.adu2394

Science Robotics

In situ foliar augmentation of multiple species for optical phenotyping and bioengineering using soft robotics

Mehmet Mert #Iman, Annika Huber, Anand K. Mishra, Sabyasachi Sen, Fumin Wang, Tiffany Lin, Georg Jander, Abraham D. Stroock, and Robert F. Shepherd

Sci. Robot. **10** (103), eadu2394. DOI: 10.1126/scirobotics.adu2394

Science Robotics (ISSN 2470-9476) is published by the American Association for the Advancement of Science. 1200 New York Avenue NW, Washington, DC 20005. The title *Science Robotics* is a registered trademark of AAAS.